PAPER • **OPEN ACCESS**

Model-based spectral causality of cardiovascular variability interactions during head-down tilt

To cite this article: Alberto Porta *et al* 2023 *Physiol. Meas.* **44** 054001

IOP Publishing Physiol. Meas. 44 (2023) 054001 https://doi.org/10.1088/1361-6579/acce1f

Physiological Measurement

IPEM Institute of Physics and Engineering in Medicine

OPEN ACCESS

RECEIVED
29 December 2022

REVISED
31 March 2023

ACCEPTED FOR PUBLICATION
18 April 2023

PUBLISHED
9 May 2023

PAPER

Model-based spectral causality of cardiovascular variability interactions during head-down tilt

Alberto Porta[1,2,*], **Beatrice Cairo**[1], **Vlasta Bari**[1,2], **Francesca Gelpi**[1], **Beatrice De Maria**[3] and **Riccardo Colombo**[4]

[1] Department of Biomedical Sciences for Health, University of Milan, Milan, Italy
[2] Department of Cardiothoracic, Vascular Anesthesia and Intensive Care, IRCCS Policlinico San Donato, San Donato Milanese, Milan, Italy
[3] IRCCS Istituti Clinici Scientifici Maugeri, Milan, Italy
[4] Department of Anesthesiology and Intensive Care Unit, ASST Fatebenefratelli Sacco, 'Luigi Sacco' Hospital, Milan, Italy
[*] Author to whom any correspondence should be addressed.

E-mail: alberto.porta@unimi.it

Keywords: causal coherence, Geweke spectral causality, vector autoregressive model, heart rate variability, arterial blood pressure, baroreflex, cardiovascular control

Abstract

Objective. Cardiovascular control mechanisms are commonly studied during baroreceptor unloading induced by head-up tilt. Conversely, the effect of a baroreceptor loading induced by head-down tilt (HDT) is less studied especially when the stimulus is of moderate intensity and using model-based spectral causality markers. Thus, this study computes model-based causality markers in the frequency domain derived via causal squared coherence and Geweke spectral causality approach from heart period (HP) and systolic arterial pressure (SAP) variability series. *Approach*. We recorded HP and SAP variability series in 12 healthy men (age: from 41 to 71 yrs, median: 57 yrs) during HDT at −25°. The approaches are compared by considering two different bivariate model structures, namely the autoregressive and dynamic adjustment models. Markers are computed in traditional frequency bands utilized in cardiovascular control analysis, namely the low frequency (LF, from 0.04 to 0.15 Hz) and high frequency (HF, from 0.15 to 0.4 Hz) bands. *Main results*. We found that: (i) the two spectral causality metrics are deterministically related but spectral causality markers exhibit different discriminative ability; (ii) HDT reduces the involvement of the baroreflex in regulating HP-SAP variability interactions in the LF band, while leaving unmodified the action of mechanical feedforward mechanisms in both LF and HF bands; (iii) this conclusion does not depend on the model structure. *Significance*. We conclude that HDT can be utilized to reduce the impact of baroreflex and to study the contribution of regulatory mechanisms different from baroreflex to the complexity of cardiovascular control in humans.

1. Introduction

Cardiac baroreflex, namely the physiological reflex inducing a significant association between heart period (HP) and arterial pressure (AP) with HP changes lagging behind AP variations, is one of the most important cardiovascular control mechanisms (Karemaker and Wesseling 2008). Characterization of the baroreflex is a fundamental issue in clinics because its derangement favors the development of disturbances that limit importantly the quality of life such as recurrent neurally-mediated syncope (Ogoh *et al* 2004, Faes *et al* 2013b). In addition, given that pacing the heart increases AP variations under orthostatic challenge (Taylor and Eckberg 1996), baroreflex buffers AP modifications with suitable HP changes, thus contributing to keep AP under control. The value of parameters describing the cardiac arm of the baroreflex is incremented by its link with the autonomic control, especially vagal circuits (Cooke *et al* 1999, De Maria *et al* 2019, Porta *et al* 2023). This link is likely to contribute to the higher predictive value of parameters describing baroreflex function when added to more classical clinical variables in risk stratification models (La Rovere *et al* 1998, Pinna *et al* 2017).

Cardiac baroreflex is usually characterized in the frequency domain via parameters such as sensitivity and latency quantifying, respectively, the HP variation per unit modification of AP (Smyth *et al* 1969, Laude *et al* 2004, Nollo *et al* 2005) and the time elapsed to observe the HP response to an imposed modification of AP (Cevese *et al* 2001, Porta *et al* 2011, Faes *et al* 2013b, Milan-Mattos *et al* 2018). Recently, these classical parameters have been complemented by indexes derived from model-based spectral causality approaches estimating the strength of the link in the time direction from systolic AP (SAP) to HP (Porta *et al* 2002, Nollo *et al* 2005, Faes *et al* 2013a, Pernice *et al* 2022). Spectral causality markers have the desirable property to be computed in the same frequency bands of more classical univariate frequency domain autonomic markers (Pomeranz *et al* 1985, Pagani *et al* 1997), namely in the low frequency (LF) band (from 0.04 to 0.15 Hz) and in the high frequency (HF) band (from 0.15 to 0.4 Hz). However, two factors might limit their more extensive application: (i) the possible dependence of the results on the technique utilized to estimate causality; (ii) the possible effect of the model structure utilized to describe the HP-SAP dynamic interactions on the final metric.

Applications of model-based spectral causality approach is mainly limited to situations of baroreceptor unloading evoked by the reduction of the venous return imposed by standing (Porta *et al* 2002, Nollo *et al* 2005, Faes *et al* 2013a, Pernice *et al* 2022). Baroreflex activation during postural maneuvers reducing venous return to the heart took the form of an increased strength of the dependence of HP on SAP in the LF band and by a greater probability to reject the null hypothesis of HP-SAP uncoupling (Nollo *et al* 2005). Scanty information was present in literature when baroreceptors were loaded. To the best of our knowledge data are limited to the application of time, or information, domain causality markers during baroreceptor loading of limited intensity utilized to simulate the effect of microgravity condition on the Earth (i.e. head-down at $-6°$) (Corbier *et al* 2020, Shankhwar *et al* 2022). These methods do not allow the computation of markers of causality in LF and HF bands and, as such, any parallel with spectral causality data during the opposite challenge, namely baroreceptor unloading, is prevented.

The aim of the study is to typify cardiac baroreflex during baroreceptor loading of moderate intensity via two model-based spectral causality approaches. We applied causal squared coherence (CK^2) (Porta *et al* 2002) and Geweke spectral causality (GSC) (Geweke 1982). GSC was selected because it is a classical model-based spectral causality metric (Geweke 1982), while CK^2 was chosen for comparison, being linked to GSC but not fully equivalent to it (Porta *et al* 2002). Two different model structures, namely the bivariate autoregressive (BAR) and the bivariate dynamic adjustment (BDA) models (Baselli *et al* 1997, Porta *et al* 2006) were utilized to describe HP-SAP variability interactions. Baroreceptor loading of moderate intensity was obtained via head-down tilt (HDT) at $-25°$ (Porta *et al* 2015a). Preliminary results were presented at the 12th meeting of the European Study Group on Cardiovascular Oscillations (Porta *et al* 2022).

2. Model-based spectral causality

2.1. Linear parametric bivariate models

Let us consider two stochastic zero mean Gaussian stationary processes Y_1 and Y_2 being collections of consecutive states $Y_1 = \{Y_{1,n},\ n = 1, \ldots, N\}$ and $Y_2 = \{Y_{2,n},\ n = 1, \ldots, N\}$ up to the time N. The linear parametric bivariate model class describes the current state $Y_{i,n}$ of Y_i, with $I = 1, 2$, as a linear combination of p past states of Y_i and p past states of Y_j,with $j = 1, 2$ and $j \neq i$, plus the current state $\Xi_{i,n}$ of an additive noise Ξ_i. Thus

$$\begin{aligned} Y_{1,n} &= \sum_{k=1}^{p} a_{11,k} \cdot Y_{1,n-k} + \sum_{k=0}^{p} a_{12,k} \cdot Y_{2,n-k-\tau_{12}} + \Xi_{1,n} \\ Y_{2,n} &= \sum_{k=0}^{p} a_{21,k} \cdot Y_{1,n-k-\tau_{21}} + \sum_{k=1}^{p} a_{22,k} \cdot Y_{2,n-k} + \Xi_{2,n}, \end{aligned} \tag{1}$$

where $a_{11,k}$, $a_{12,k}$, $a_{21,k}$ and $a_{22,k}$ are constant coefficients and τ_{12} and τ_{21} are the latencies of the action of Y_2 onto Y_1 and vice versa respectively. The setting $\tau_{12} = 0$ and $\tau_{21} = 0$ must be prevented to avoid the creation of a loop without delay (Baselli *et al* 1997, Porta *et al* 2002). Immediate effects between Y_1 and Y_2 can be described by setting $\tau_{12} = 0$ with $\tau_{21} \neq 0$ or $\tau_{21} = 0$ with $\tau_{12} \neq 0$ according to physiological considerations about the rapidity of cross-actions. The linear parametric bivariate class is usually referred to as BAR if $\Xi_{i,n} = \Omega_{i,n}$ is the current state of a zero mean Gaussian white noise Ω_i with variance λ_i^2, while it is usually referred to BDA if $\Xi_{i,n}$ is the current state of a zero mean Gaussian autoregressive (AR) process Ξ_i with

$$\Xi_{i,n} = \sum_{k=1}^{p} d_{i,k} \cdot \Xi_{i,n-k} + \Omega_{i,n}, \tag{2}$$

that might feature rhythms according to the set of p constant coefficients $d_{i,k}$. We hypothesize that Ω_1 and Ω_2 are uncorrelated each other, thus cross-covariance between Ω_1 and Ω_2 is 0 at any lag including lag zero.

2.2. Spectral matrix of the linear parametric bivariate models

The application of the z-transform to (1) leads to z-domain representation of the bivariate process

$$\boldsymbol{Y}(z) = \boldsymbol{A}(z) \cdot \boldsymbol{Y}(z) + \boldsymbol{\Xi}(z), \tag{3}$$

with $\boldsymbol{Y}(z) = |\ Y_1(z) \quad Y_2(z)\ |^{\mathrm{T}}$, $\boldsymbol{\Xi}(z) = |\ \Xi_1(z) \quad \Xi_2(z)\ |^{\mathrm{T}}$, and

$$\boldsymbol{A}(z) = \begin{vmatrix} A_{11}(z) & A_{12}(z) \\ A_{21}(z) & A_{22}(z) \end{vmatrix}, \tag{4}$$

where $\boldsymbol{Y}(z)$ and $\boldsymbol{\Xi}(z)$ are the z-transforms of $\boldsymbol{Y} = |\ Y_1 \quad Y_2\ |^{\mathrm{T}}$ and $\boldsymbol{\Xi} = |\ \Xi_1 \quad \Xi_2\ |^{\mathrm{T}}$ respectively, and $A_{11}(z) = \sum_{k=1}^{p} a_{11,k} \cdot z^{-k}$, $A_{12}(z) = \sum_{k=0}^{p} a_{12,k} \cdot z^{-k-\tau_{12}}$, $A_{21}(z) = \sum_{k=0}^{p} a_{21,k} \cdot z^{-k-\tau_{21}}$ and $A_{22}(z) = \sum_{k=1}^{p} a_{22,k} \cdot z^{-k}$ are polynomials with constant coefficients in z^{-1} and T is the transposition operator. In the case of the BAR model $\boldsymbol{\Xi}(z) = \Omega(z) = |\ \Omega_1(z) \quad \Omega_2(z)\ |^{\mathrm{T}}$, while in the case of the BDA structure $\boldsymbol{\Xi}(z) = \mathrm{diag}|[1 - D_i(z)]^{-1}| \cdot \Omega(z)$, where $D_i(z) = \sum_{k=1}^{p} d_{i,k} \cdot z^{-k}$, with $i = 1, 2$, and $\mathrm{diag}|\cdot|$ is a diagonal 2×2 matrix having $[1 - D_i(z)]^{-1}$ over the main diagonal and 0 out of it.

The transfer function matrix $\boldsymbol{H}(z)$ links $\Omega(z)$ to $\boldsymbol{Y}(z)$ as

$$\boldsymbol{Y}(z) = \boldsymbol{H}(z) \cdot \Omega(z) \tag{5}$$

with $\boldsymbol{H}(z) = [\mathbf{I} - \boldsymbol{A}(z)]^{-1}$ in the case of the BAR model and $\boldsymbol{H}(z) = [\mathbf{I} - \boldsymbol{A}(z)]^{-1} \cdot \mathrm{diag}|[1 - D_i(z)]^{-1}|$ in the case of the BDA structure, where $\mathbf{I}$ is 2×2 identity matrix. Under the hypothesis of whiteness of Ω_1 and Ω_2 and their uncorrelation, the spectral density matrix $\boldsymbol{S}(f)$ can be computed as

$$\boldsymbol{S}(f) = T \cdot \boldsymbol{H}(z) \cdot \boldsymbol{\Lambda} \cdot \boldsymbol{H}^{\mathrm{T}}(z^{-1})|_{z=\mathrm{e}^{\mathrm{j}2\pi \cdot f \cdot T}}, \tag{6}$$

where T is the sampling period and $\boldsymbol{\Lambda}$ is the 2×2 variance matrix of Ω with $\boldsymbol{\Lambda} = \mathrm{diag}|\lambda_i^2|$ reporting the variances of the zero mean Gaussian white noises over the main diagonal and 0 out of it. In our application sampling period T is the average HP (μ_{HP}) assuming that the values of the series are evenly sampled at a rate of μ_{HP}^{-1}. Thus, Nyquist frequency f_N is $0.5 \cdot \mu_{HP}^{-1}$.

2.3. Model-based parametric squared coherence (K^2)

The BAR representation leads to the power spectral density $S_{ii}(f)$ of Y_i with $i = 1, 2$ given by

$$S_{11}(f) = T \cdot \frac{[1 - A_{22}(z)] \cdot [1 - A_{22}(z^{-1})] \cdot \lambda_1^2}{\Delta(z) \cdot \Delta(z^{-1})} + T \cdot \frac{A_{12}(z) \cdot A_{12}(z^{-1}) \cdot \lambda_2^2}{\Delta(z) \cdot \Delta(z^{-1})}\Bigg|_{z=\mathrm{e}^{\mathrm{j}2\pi \cdot f \cdot T}}, \tag{7}$$

$$S_{22}(f) = T \cdot \frac{A_{21}(z) \cdot A_{21}(z^{-1}) \cdot \lambda_1^2}{\Delta(z) \cdot \Delta(z^{-1})} + T \cdot \frac{[1 - A_{11}(z)] \cdot [1 - A_{11}(z^{-1})] \cdot \lambda_2^2}{\Delta(z) \cdot \Delta(z^{-1})}\Bigg|_{z=\mathrm{e}^{\mathrm{j}2\pi \cdot f \cdot T}}, \tag{8}$$

and to the cross-power spectral density $S_{12}(f)$ given by

$$S_{12}(f) = T \cdot \frac{[1 - A_{22}(z)] \cdot A_{21}(z^{-1}) \cdot \lambda_1^2}{\Delta(z) \cdot \Delta(z^{-1})} + T \cdot \frac{A_{12}(z) \cdot [1 - A_{11}(z^{-1})] \cdot \lambda_2^2}{\Delta(z) \cdot \Delta(z^{-1})}\Bigg|_{z=\mathrm{e}^{\mathrm{j}2\pi \cdot f \cdot T}}, \tag{9}$$

while the BDA model leads to the power spectral density $S_{ii}(f)$ of Y_i with $i = 1, 2$ given by

$$S_{11}(f) = T \cdot \frac{[1 - A_{22}(z)] \cdot [1 - A_{22}(z^{-1})] \cdot \lambda_1^2}{\Delta(z) \cdot \Delta(z^{-1}) \cdot [1 - D_1(z)] \cdot [1 - D_1(z^{-1})]} + T \cdot \frac{A_{12}(z) \cdot A_{12}(z^{-1}) \cdot \lambda_2^2}{\Delta(z) \cdot \Delta(z^{-1}) \cdot [1 - D_2(z)] \cdot [1 - D_2(z^{-1})]}\Bigg|_{z=\mathrm{e}^{\mathrm{j}2\pi \cdot f \cdot T}}, \tag{10}$$

$$S_{22}(f) = T \cdot \frac{A_{21}(z) \cdot A_{21}(z^{-1}) \cdot \lambda_1^2}{\Delta(z) \cdot \Delta(z^{-1}) \cdot [1 - D_1(z)] \cdot [1 - D_1(z^{-1})]} + T \cdot \frac{[1 - A_{11}(z)] \cdot [1 - A_{11}(z^{-1})] \cdot \lambda_2^2}{\Delta(z) \cdot \Delta(z^{-1}) \cdot [1 - D_2(z)] \cdot [1 - D_2(z^{-1})]}\Bigg|_{z=\mathrm{e}^{\mathrm{j}2\pi \cdot f \cdot T}}, \tag{11}$$

and to the cross-power spectral density $S_{12}(f)$ given by

$$S_{12}(f) = T \cdot \frac{[1 - A_{22}(z)] \cdot A_{21}(z^{-1}) \cdot \lambda_1^2}{\Delta(z) \cdot \Delta(z^{-1}) \cdot [1 - D_1(z)] \cdot [1 - D_1(z^{-1})]} + T \cdot \frac{A_{12}(z) \cdot [1 - A_{11}(z^{-1})] \cdot \lambda_2^2}{\Delta(z) \cdot \Delta(z^{-1}) \cdot [1 - D_2(z)] \cdot [1 - D_2(z^{-1})]}\Bigg|_{z=\mathrm{e}^{\mathrm{j}2\pi \cdot f \cdot T}}, \tag{12}$$

with $\Delta(z) = [1 - A_{11}(z)] \cdot [1 - A_{22}(z)] - A_{12}(z) \cdot A_{21}(z)$. Since over the unit circle $z = e^{j2\pi \cdot f \cdot T}$, polynomials of real coefficients lead to $\Delta(z)^* = \Delta(z^{-1})$, $A_{ij}(z)^* = A_{ij}(z^{-1})$, $[1 - A_{ii}(z)]^* = [1 - A_{ii}(z^{-1})]$, and $[1 - D_i(z)]^* = [1 - D_i(z^{-1})]$ where * is the complex conjugation operator, $\Delta(z) \cdot \Delta(z^{-1}) = |\Delta(z)|^2$, $A_{ij}(z) \cdot A_{ij}(z^{-1}) = |A_{ij}(z)|^2$, $[1 - A_{ii}(z)] \cdot [1 - A_{ii}(z^{-1})] = |1 - A_{ii}(z)|^2$ and $[1 - D_i(z)] \cdot [1 - D_i(z^{-1})] = |1 - D_i(z)|^2$, where $|\cdot|$ takes the modulus of the complex number, thus simplifying the computation. Equations (7), (8), (10) and (11) represent the typical factorization of power spectral density $S_{ii}(f)$ of Y_i into partial power spectral density $S_{ii,1}(f)$ due to Ω_1 and $S_{ii,2}(f)$ due to Ω_2 and equations (9) and (12) the typical factorization of power cross-spectral density $S_{12}(f)$ into partial power cross-spectral density $S_{12,1}(f)$ due to Ω_1 and $S_{12,2}(f)$ due to Ω_2 (Baselli *et al* 1997, Porta *et al* 2006).

Since squared coherence K^2 between Y_1 and Y_2 is defined as

$$K_{12}^2(f) = \frac{|S_{12}(f)|^2}{S_{11}(f) \cdot S_{22}(f)}, \tag{13}$$

equations (7), (8) and (9) allow the computation of $K_{12}^2(f)$ based on the BAR representation and (10), (11) and (12) that of $K_{12}^2(f)$ based on the BDA one. Since $S_{12}^*(f) = S_{21}(f)$, $K_{21}^2(f) = K_{12}^2(f)$.

2.4. Model-based parametric CK^2

K^2 is turned out to be CK^2 by artificially opening the closed loop (Porta *et al* 2002). Practically, the CK^2 from Y_j to Y_i, with $i, j = 1, 2$ and $i \neq j$, is computed from K^2 by nullifying the polynomial describing the causal relationship over the reverse causal direction, namely from Y_i to Y_j, as

$$CK_{Y_j \to Y_i}^2(f) = K_{ij}^2(f)|_{A_{ji}(z)=0}. \tag{14}$$

Thus, in the case of BAR, CK^2 is

$$CK_{Y_j \to Y_i}^2(f) = \frac{|A_{ij}(z)|^2 \cdot \lambda_j^2}{|1 - A_{jj}(z)|^2 \cdot \lambda_i^2 + |A_{ij}(z)|^2 \cdot \lambda_j^2}\Bigg|_{z=e^{j2\pi \cdot f \cdot T}} \tag{15}$$

and, in the case of BDA, CK^2 is

$$CK_{Y_j \to Y_i}^2(f) = \frac{|A_{ij}(z)|^2 \cdot |1 - D_i(z)|^2 \cdot \lambda_j^2}{|1 - A_{jj}(z)|^2 \cdot |1 - D_j(z)|^2 \cdot \lambda_i^2 + |A_{ij}(z)|^2 \cdot |1 - D_i(z)|^2 \cdot \lambda_j^2}\Bigg|_{z=e^{j2\pi \cdot f \cdot T}}. \tag{16}$$

A closer look to the (15) and (16) allows one to link them to the partial power spectral density $S_{ii,j}(f)$, with $i \neq j$, and to the power spectral density $S_{ii}(f)$. The final marker is computed by sampling $CK_{Y_j \to Y_i}^2(f)$ in correspondence of its peak within the frequency band of interest (Porta *et al* 2002).

2.5. GSC and its relationship with CK^2

The GSC exploits the observation that the fractional contribution of $S_{ii,i}(f)$ to $S_{ii}(f)$ tends to 0 with the relevance of the impact of the link from Y_j to Y_i with $i \neq j$. Thus

$$\mathrm{GSC}_{Y_j \to Y_i}(f) = -\log \frac{S_{ii,i}(f)}{S_{ii}(f)}, \tag{17}$$

where $\log(\cdot)$ is the natural logarithm, was taken as a measure of the strength of the causal link from Y_j to Y_i in the frequency domain (Geweke 1982). $\mathrm{GSC}_{Y_j \to Y_i}(f)$ is integrated over the frequency band of interest (Geweke 1982). Given that $CK_{Y_j \to Y_i}^2(f)$ is the ratio of $S_{ii,j}(f)$ to $S_{ii}(f)$, and $S_{ii}(f) = S_{ii,i}(f) + S_{ii,j}(f)$ with $i, j = 1, 2$ and $i \neq j$, then $\mathrm{GSC}_{Y_j \to Y_i}(f) = -\log[1 - CK_{Y_j \to Y_i}^2(f)]$. This relationship strictly holds between functions but, in general, it does not hold between markers derived from the functions. Therefore, different abilities between CK^2 and GSC markers in assessing the strength of the causal relationship can be exclusively attributed to the procedure applied to extract the final marker from the original metrics, namely sampling in the case of $CK_{Y_j \to Y_i}^2(f)$ and integration over a given range of frequencies in the case of $\mathrm{GSC}_{Y_j \to Y_i}(f)$.

3. Experimental protocol and data analysis

3.1. Experimental protocol

The study exploited an historical database built to study the autonomic response to baroreceptor loading in healthy individuals (Porta *et al* 2015a). The protocol adhered to the principles of the Declaration of Helsinki for medical research involving human subjects. The human research and ethical review board of the 'Luigi Sacco' Hospital, Milan, Italy approved the protocol. Written signed informed consent was obtained from all subjects.

We studied 12 healthy men (age: 41–71 yrs; median: 57 yrs). The healthy status of the subjects was confirmed via the careful assessment of the personal health record and clinical examination. The subjects were free of any medication and were invited to avoid strenuous physical exercise and consumption of caffeine or alcoholic beverages in the 24 h before the experimental session. Sessions comprised simultaneous recordings of electrocardiogram (ECG) from lead II and noninvasive finger volume-clamped AP (Nexfin, BMEYE, Amsterdam, The Netherlands). Signals were sampled at 400 Hz. AP was measured noninvasively from the middle finger of the dominanthand. The subject's dominant arm was fixed to the thorax to maintain the hand at the heart level. The non-dominant arm was aligned to the trunk. AP was cross-calibrated on an individual basis with a measurement taken at the onset of the experimental session with a sphygmomanometer. The autocalibration procedure of the AP device was switched off after the first automatic calibration at the onset of the session. The subjects were not allowed to talk during the protocol. Each experimental session comprised 10 min of baseline at rest in supine position (REST) followed by 10 min during HDT with a table inclination of $-25°$. A period of stabilization was allowed after having instrumented the subject and before starting signal acquisition. The head was maintained it in a neutral position by a headrest. During the protocol, the subjects breathed according to a metronome at 16 breaths·min^{-1}. The first three minutes of recordings during HDT were skipped to avoid transient variations of the physiological variables.

3.2. Extraction of the beat-to-beat variability series

The time interval between two consecutive *R*-wave peaks of the ECG was taken as the *n*th HP (HP_n). The maximum AP within HP_n was identified as the *n*th SAP (SAP_n). Detections of *R*-wave apexes from the ECG and systolic peaks from the AP were visually checked. Standard procedures to insert missed identifications, to correct and reinsert eventual misdetections and to limit the effect of arrhythmic beats were applied (Porta *et al* 2015a). A few isolated ectopic beats were detected, but their number was always less than 5% of the total length of the sequence. As the focus of the study was the characterization of short-term HP-SAP variability interactions, the analysis was carried out over sequences of 256 consecutive synchronous HP and SAP values taken in a random position within REST and HDT sessions. Stationarity of mean and variance of HP and SAP series was tested (Magagnin *et al* 2011).

3.3. Time and frequency domain markers

In the time domain we computed the mean and variance of HP and SAP denoted as μ_{HP}, σ^2_{HP}, μ_{SAP} and σ^2_{SAP} and expressed in, respectively, ms, ms^2, mmHg and mmHg^2. Frequency domain analysis was carried out via traditional parametric AR method. The coefficients of the AR model and the variance of the white noise were estimated directly from the series by solving the least squares problem via Levinson–Durbin recursion (Baselli *et al* 1997). The number of coefficients *p* was chosen according to the Akaike's figure of merit in the range from 8 to 14 (Akaike 1974). Power spectral density was computed from the transfer function of the AR process and from the variance of the white noise according to univariate version of (6) (Baselli *et al* 1997). The power spectral density was factorized into a sum of terms, referred to as spectral components, the sum of which provides the entire power spectral density (Baselli *et al* 1997). Spectral components were labelled as LF, or HF, if their central frequencies, converted in Hz by dividing the normalized frequency expressed in cycles·beat^{-1} by the μ_{HP}, dropped into the LF, or HF, band. If multiple spectral components belonged to the same frequency band, their powers were summed up. The HP power in the HF band, expressed in ms^2 and denoted as HF_{HP}, was taken as a marker of vagal modulation directed to the heart (Pomeranz *et al* 1985) and SAP power in the LF band, expressed in mmHg^2 and denoted as LF_{SAP}, was utilized as a marker of sympathetic modulation directed to the vessels (Pagani *et al* 1997).

3.4. Model-based frequency domain spectral causality indexes

Model-based frequency domain spectral causality markers were computed over HP and SAP series. Both time directions of interactions, namely along the baroreflex, from SAP to HP, and along the mechanical feedforward pathway, from HP to SAP, were considered. Indexes were computed via CK[2] and GSC approaches in the LF and HF bands. Both BAR and BDA classes were exploited to describe the HP-SAP dynamic interactions. Series were linearly detrended and normalized to have unit variance before computing causality markers. Traditional least squares technique was applied to identify the coefficients of the BAR model, while those of the BDA model were estimated via generalized least squares method (Baselli *et al* 1997). While traditional least squares approach allows a closed form solution of the identification problem, generalized least squares method is an iterative method monitoring the prediction error variance at each iteration. Iterative procedure continued until the absolute value of the fractional between-iteration decrease of the prediction error variance was below 0.001. Traditional and generalized least squares problems were solved via the Cholesky decomposition method. The model order was optimized via the Akaike information criterion for multivariate processes in the range from 5 to

12 (Akaike 1974). The latency from SAP to HP and from HP to SAP was assigned to 0 and 1 beat respectively (Porta *et al* 2002). Markers of CK^2 were computed by sampling CK^2 in correspondence of its peak in the LF and HF bands (Porta *et al* 2002). The markers of CK^2 were labelled $CK^2_{SAP\rightarrow HP}$(LF) and $CK^2_{SAP\rightarrow HP}$(HF) from SAP to HP and $CK^2_{HP\rightarrow SAP}$(LF) and $CK^2_{HP\rightarrow SAP}$(HF) from HP to SAP. Indexes of GSC were calculated by integrating GSC over LF and HF bands (Geweke 1982, Pernice *et al* 2022). The markers of GSC were labelled $GSC_{SAP\rightarrow HP}$(LF) and $GSC_{SAP\rightarrow HP}$(HF) from SAP to HP and $GSC_{HP\rightarrow SAP}$(LF) and $GSC_{HP\rightarrow SAP}$(HF) from HP to SAP.

3.5. Assessing the significance of frequency domain spectral causality indexes

Surrogate data test was applied to reject the null hypothesis of uncoupling between HP and SAP that results from an unsignificant causal link between the two series. One hundred surrogate series couples were generated from each original HP and SAP pair in any experimental condition. The surrogate series preserved the amplitude distribution and power spectral density of the original series, while phases were substituted with uniformly distributed random numbers ranging from 0 to 2π. We exploited an iteratively refined procedure to generate surrogate pairs (Schreiber and Schmitz 1996). The procedure maintained exactly the original amplitude distribution of the series, while the power spectrum was the best approximation of the initial power spectrum given 100 iterates. The uncoupling between the HP and SAP surrogates was assured using two independent random phase sequences (Palus 1997). The length of the series (i.e. 256) allowed us to speed up the construction of surrogates via fast Fourier transform. CK^2 and GSC markers were computed over the 100 surrogate pairs by imposing the model order optimized over the original pairs. The 95th percentile of their distribution was computed. The null hypothesis of uncoupling was rejected if the marker computed over the original series was above the 95th percentile of the distribution of the frequency domain causality indexes derived from surrogates. The percentage of subjects featuring a rejection of the null hypothesis of uncoupling was monitored in each frequency band.

3.6. Statistical analysis

Normality was tested via the Shapiro–Wilk test. The influence of HDT over time and frequency domain parameters was checked via paired t test, or Wilcoxon signed rank test when appropriate. Two-way repeated measures analysis of variance (one factor repetition, Holm–Sidak test for multiple comparisons) was applied to model-based spectral causality markers to assess the effect of HDT within the same model class (i.e. BAR or BDA models) and the difference between model classes within the same experimental condition (i.e. REST or HDT). Data are expressed as mean $\pm$ standard deviation. The impact of the model structure and HDT was assessed via $\chi 2$ test (McNemar's test) applied to the proportion of subjects featuring the rejection of the null hypothesis of uncoupling. The level of significance of the test was lowered according to the number of comparisons (i.e. 4) to account for the multiple comparison issue. The same test was applied to check the impact of HDT regardless of the model structure after pooling together results obtained from the application of BAR and BDA. In this specific case the level of significance was not lowered because there is only one comparison. Statistical analysis was performed with a commercial statistical software (Sigmaplot v.14.0, Systat Software, San Jose, CA, USA). The level of statistical significance of all the tests was set to 0.05.

4. Results

Time domain markers were not affected by HDT with μ_{HP}, σ^2_{HP}, μ_{SAP} and σ^2_{SAP} equal to 934 ± 103 ms, 1096 ± 756 ms^2, 127 ± 21 mmHg and 23 ± 11 mmHg^2 at REST and to 951 ± 114 ms, 1012 ± 574 ms^2, 131 ± 22 mmHg and 20 ± 15 mmHg^2 during HDT. During HDT frequency domain analysis indicated that HF_{HP} increased (i.e. 154 ± 135 ms^2 versus 219 ± 148 ms^2), while LF_{SAP} decreased (i.e. 8 ± 8 mmHg^2 versus 4 ± 3 mmHg^2).

The grouped vertical bar graphs of figure 1 show the percentage of rejections of the null hypothesis of uncoupling from SAP to HP (figures 1(a), (c)) and from HP to SAP (figures 1(b), (d)) derived from the surrogate data test applied to CK^2 markers in the LF (figures 1(a), (b)) and HF (figures 1(c), (d)) bands. The percentages are computed according to the description of the HP-SAP dynamic interactions given by BAR (black bars) and BDA (white bars) models and reported as a function of the experimental condition (i.e. REST and HDT). Regardless of the frequency band (i.e. LF or HF) and direction of the interactions (i.e. from SAP to HP or vice versa) the percentage of rejections of the null hypothesis of uncoupling did not vary with the model structure and experimental condition.

The simple vertical bar graphs of figure 2 show the percentage of rejections of the null hypothesis of uncoupling from SAP to HP (figures 2(a), (c)) and from HP to SAP (figures 2(b), (d)) derived from the surrogate data test applied to CK^2 markers in the LF (figures 2(a), (b)) and HF (figures 2(c), (d)) bands. Percentages are computed after pooling together the results of surrogate data test regardless of the model structure (i.e. BAR or

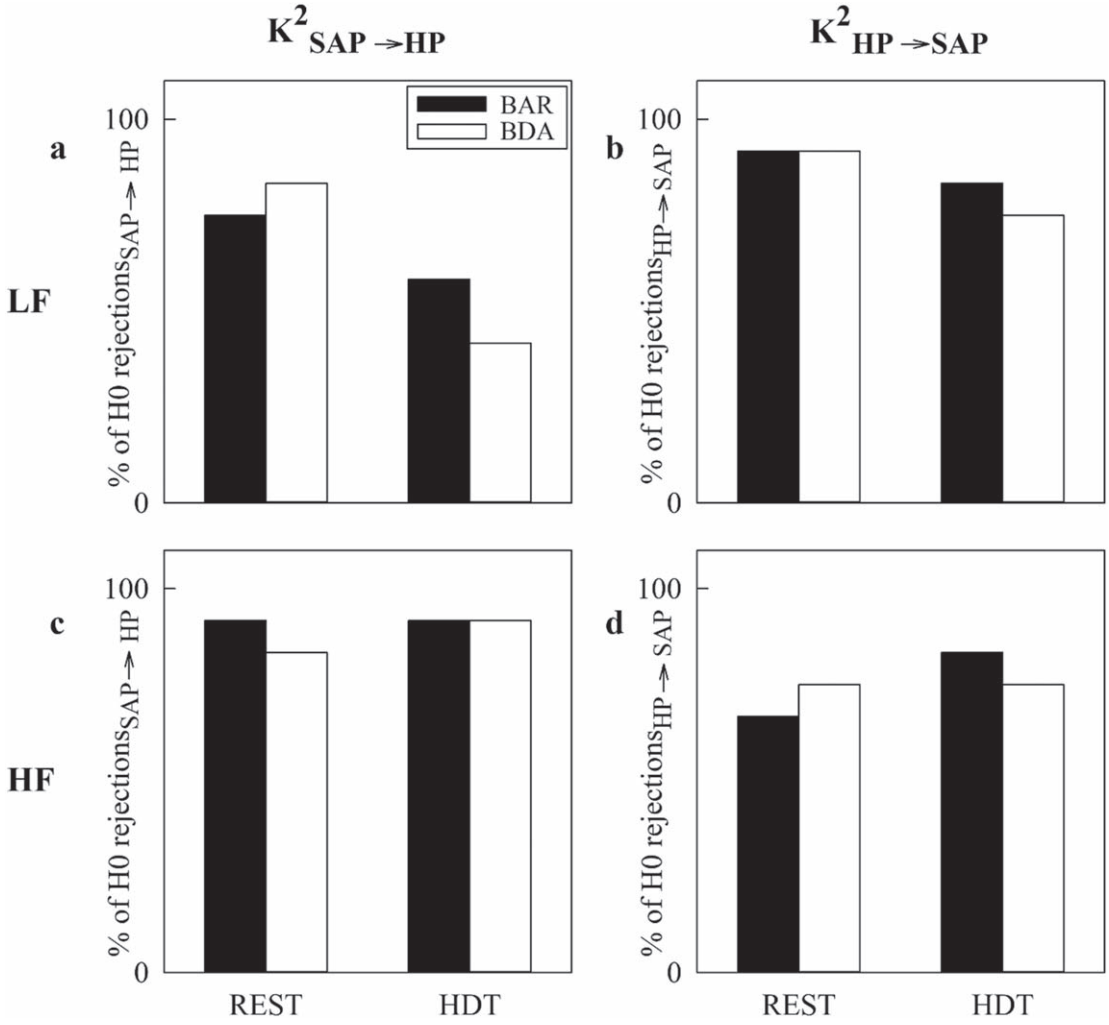

Figure 1. The grouped vertical bar graphs show the percentage of rejections of the null hypothesis of uncoupling from SAP to HP (a), (c) and from HP to SAP (b), (d) computed in the LF (a), (b) and HF (c), (d) bands. The percentages are calculated using CK^2. Results are derived according to the description of the HP-SAP dynamic interactions given by BAR (black bars) and BDA (white bars) models as a function of the experimental condition (i.e. REST and HDT).

BDA) and shown as a function of the experimental condition (i.e. REST and HDT). The percentage of rejections of the null hypothesis of uncoupling significantly decreased during HDT in direction from SAP to HP in the LF band (figure 2(a)), thus indicating a decreased strength of the dependence of HP on SAP in the LF band. Conversely, HDT did not affect the percentage of rejections of the null hypothesis of uncoupling in the HF band (figure 2(c)) and in time direction from HP to SAP regardless of the frequency band (figures 2(b), (d)).

Figure 3 has the same structure as figure 1, but it shows the percentage of rejections of the null hypothesis of uncoupling derived from the surrogate data test applied to GSC markers. As in figure 1 the percentage of rejections of the null hypothesis of uncoupling remained constant with the model structure and experimental condition and this result held regardless of the frequency band and direction of the interactions.

Figure 4 has the same structure as figure 2, but it shows the percentage of rejections of the null hypothesis of uncoupling as derived from the surrogate data test applied to GSC markers. The percentage of rejections of the null hypothesis of uncoupling did not vary with HDT and this result held regardless of the frequency band and direction of the interactions.

Markers of the strength of the causal link in LF and HF bands are reported in table 1. The indexes were computed in the direction from SAP to HP and vice versa at REST and during HDT according to the BAR and BDA models. Data were averaged over all the subjects regardless of the outcome of the surrogate test. The effect of HDT was significant solely over $CK^2_{SAP\rightarrow HP}$(LF): indeed, regardless of the model structure $CK^2_{SAP\rightarrow HP}$(LF) decreased during HDT. GSC markers were not affected either by the experimental challenge or model structure.

Figure 5 shows the scatter plots in the plane (GSC, CK^2). Each open circle corresponds to a pair (GSC, CK^2) in an assigned individual. Data are pooled together regardless of the experimental condition (i.e. REST or HDT) and type of model (i.e. BAR or BDA). The scatter plots are relevant to markers from SAP to HP (figures 5(a), (c))

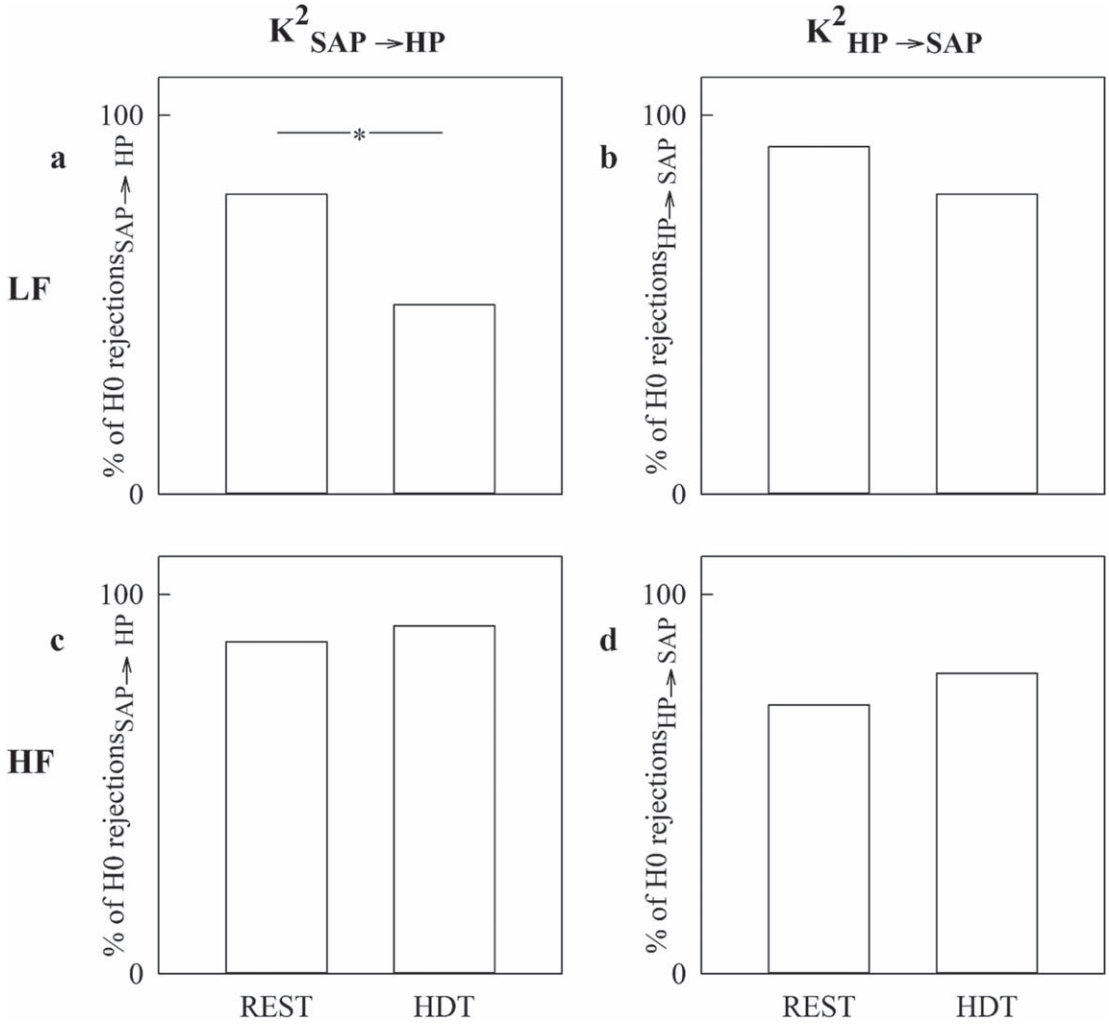

Figure 2. The simple vertical bar graphs show the percentage of rejections of the null hypothesis of uncoupling from SAP to HP (a), (c) and from HP to SAP (b), (d) computed in the LF (a), (b) and HF (c), (d) bands. The percentages are calculated using CK^2 after pooling together the results of the surrogate test regardless of the model structure (i.e. BAR or BDA). Results are shown as a function of the experimental condition (i.e. REST and HDT). The symbol * indicates a significant between-condition change with $p < 0.05$.

and from HP to SAP (figures 5(b), (d)) computed in the LF (figures 5(a), (b)) and HF (figures 5(c), (d)) bands. The scatter plots highlight the association between GSC and CK^2 indexes resulting from the deterministic relationship between GSC and CK^2 function suggested by section 2.5. The variability of the circles in the scatter plots is the sole consequence on how the final marker was computed from the original metric.

5. Discussion

The major findings of the study can be summarized as follows: (i) bivariate model-based CK^2 and GSC metrics were deterministically related but spectral causality markers exhibited different discriminative ability (i.e. statistical power); (ii) HDT reduced the involvement of the baroreflex in regulating HP-SAP variability interactions in the LF band, while leaving unmodified the action of mechanical feedforward mechanisms in both LF and HF bands; (iii) this conclusion did not depend on the model structure.

5.1. Impact of the model class and relationship between CK^2 and GSC markers

The most original methodological part of the study is the comparison between linear bivariate parametric model classes utilized to assess spectral causality markers, namely BAR and BDA (Baselli *et al* 1997, Porta *et al* 2006). The BAR class is the most widely utilized class of linear bivariate parametric models not only to compute causality markers in the frequency domain (Akaike 1968, Baccala *et al* 1998, Baccala and Sameshima 2001, Kaminski *et al* 2001, Porta *et al* 2002, Nollo *et al* 2005, Chen *et al* 2006, Chicharro 2011, Faes *et al* 2013a, Barnett and Seth 2014, Porta and Faes 2016, Pernice *et al* 2022) but also to calculate causality indexes in time and

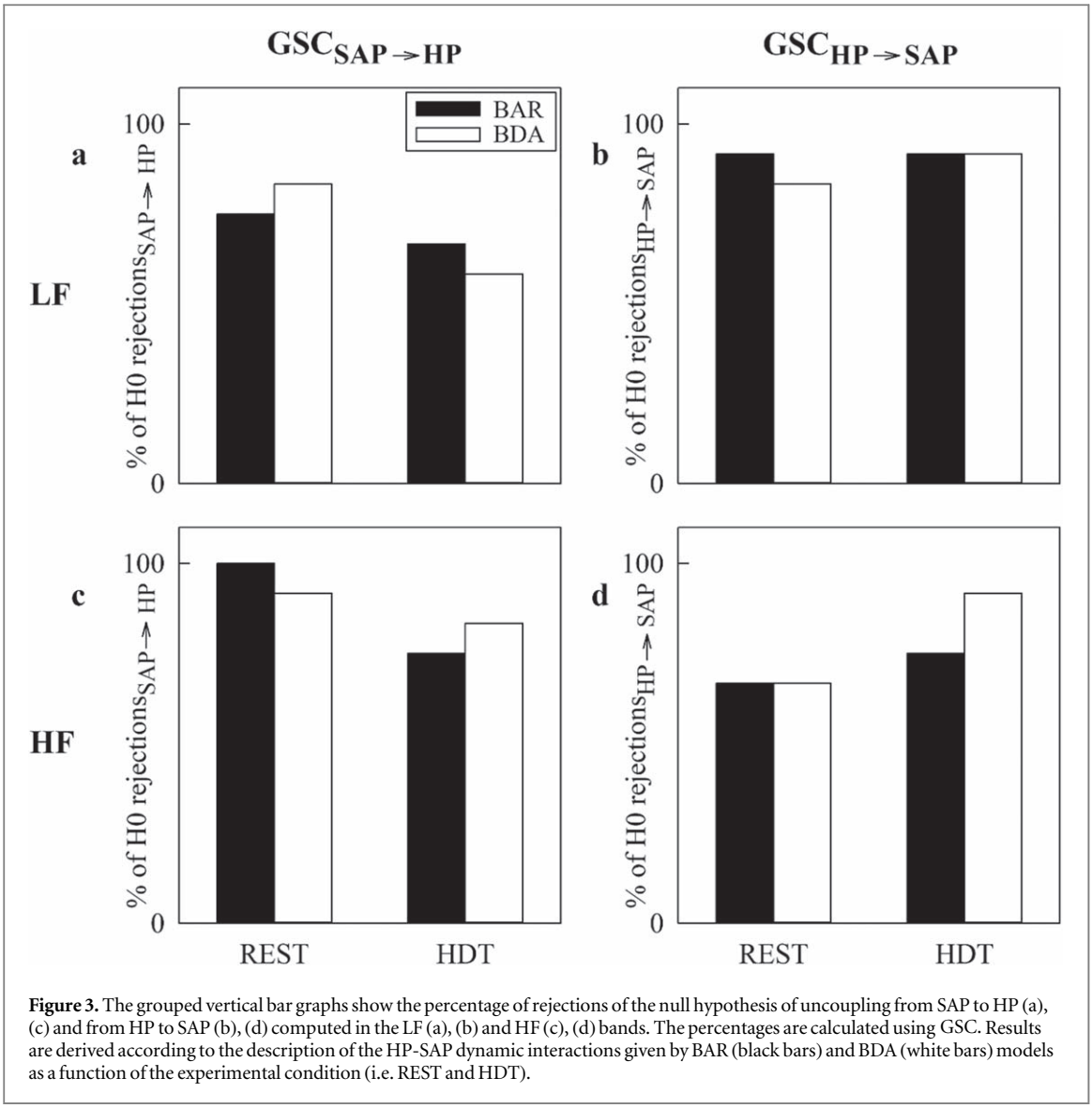

Figure 3. The grouped vertical bar graphs show the percentage of rejections of the null hypothesis of uncoupling from SAP to HP (a), (c) and from HP to SAP (b), (d) computed in the LF (a), (b) and HF (c), (d) bands. The percentages are calculated using GSC. Results are derived according to the description of the HP-SAP dynamic interactions given by BAR (black bars) and BDA (white bars) models as a function of the experimental condition (i.e. REST and HDT).

information domains (Barnett *et al* 2009, Eichler 2013, Porta *et al* 2013b, Porta *et al* 2015b, Corbier *et al* 2020, Shankhwar *et al* 2022). Conversely, the BDA class is less frequently exploited (Baselli *et al* 1997, Porta *et al* 2006) as a likely consequence of its more involved identification procedure requiring generalized least squares approach. This identification method is based on the solution of two ordinary least squares problems in sequence and iteratively. The original data are filtered using the coefficients of the AR noise under an initial guess and the coefficients of the BAR network are estimated from the filtered series. The parameters of the BAR network are utilized to generate the residuals that are fitted with an AR model. The coefficients of the AR noise are updated to filter the original data at the next iteration. The procedure continues until the prediction error variance ceases to decrease with the iteration number. The BDA model was found useful to describe HP and SAP oscillations that are not generated by the interaction between the variability series, but they are the effect of the activity of external oscillators impinging the BAR network (Baselli *et al* 1994, Baselli *et al* 1997, Porta *et al* 2006). Since the results obtained from BAR and BDA models are similar, we conclude that baroreflex and mechanical feedforward pathway can explain HP and SAP variability both at REST and during HDT without the need to describe external, colored, inputs. This conclusion might not hold under pharmacological challenge or in pathological subjects (Porta *et al* 2000).

In addition, the present study provides the explicit expression of CK^2 and GSC and their relationship as well as the comparison of indexes derived from CK^2 and GSC. The deterministic relationship between CK^2 and GSC, highlighted in section 2.5, does not hold in general between markers derived from these metrics. Therefore, we attribute the different statistical power between causality markers, with CK^2 markers slightly more powerful in detecting the effect of HDT via a surrogate data test, solely to the procedure utilized to finally compute spectral causality indexes from the frequency domain metric.

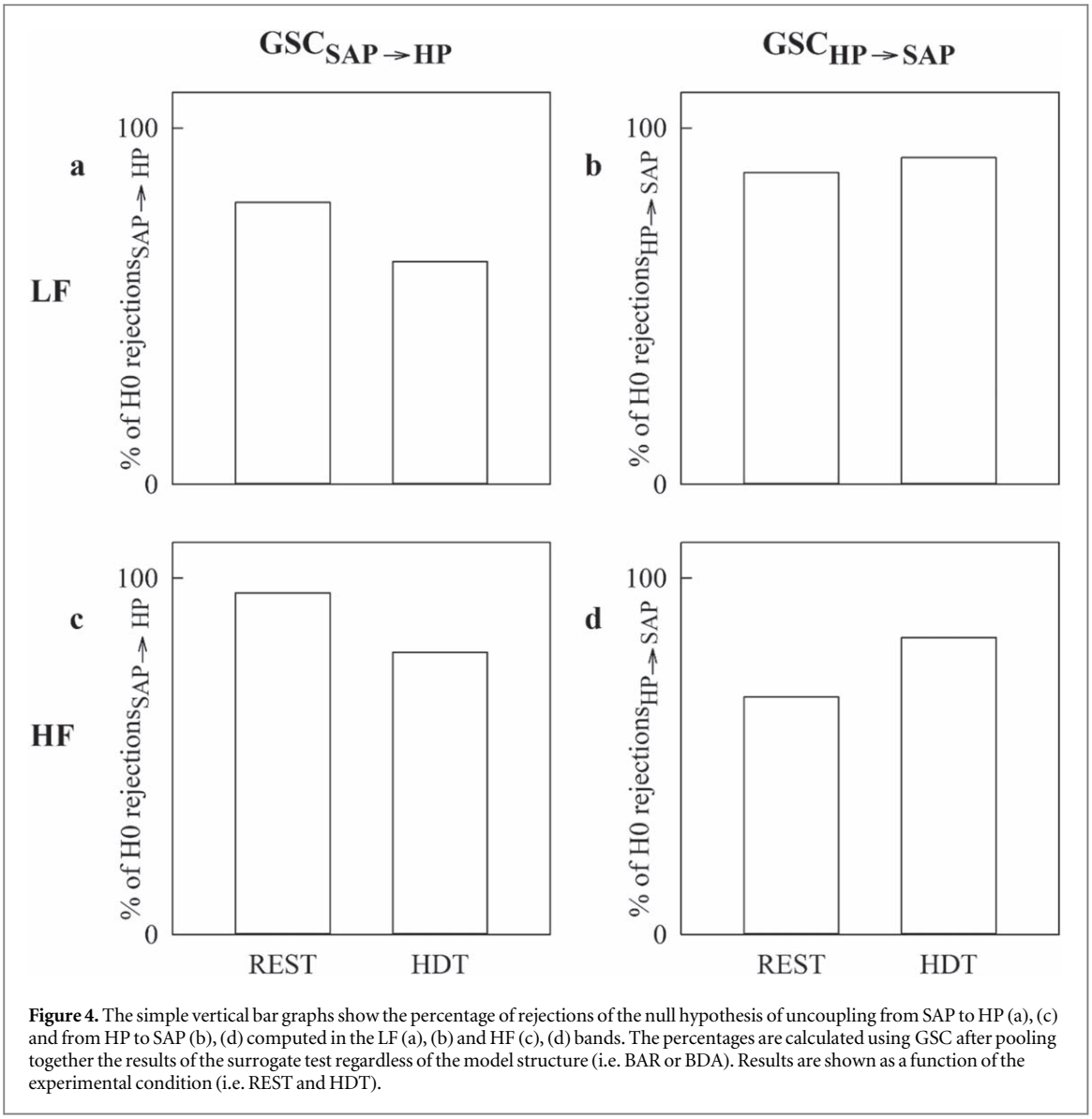

Figure 4. The simple vertical bar graphs show the percentage of rejections of the null hypothesis of uncoupling from SAP to HP (a), (c) and from HP to SAP (b), (d) computed in the LF (a), (b) and HF (c), (d) bands. The percentages are calculated using GSC after pooling together the results of the surrogate test regardless of the model structure (i.e. BAR or BDA). Results are shown as a function of the experimental condition (i.e. REST and HDT).

Table 1. Spectral causality markers from SAP to HP and vice versa in LF and HF bands assessed via BAR and BDA models.

Spectral causality marker	BAR		BDA	
	REST	HDT	REST	HDT
$CK^2_{SAP\rightarrow HP}$(LF)	0.39 ± 0.15	$0.29 \pm 0.18^*$	0.44 ± 0.16	$0.30 \pm 0.16^*$
$CK^2_{HP\rightarrow SAP}$(LF)	0.46 ± 0.18	0.53 ± 0.22	0.48 ± 0.15	0.57 ± 0.20
$CK^2_{SAP\rightarrow HP}$(HF)	0.50 ± 0.18	0.36 ± 0.20	0.51 ± 0.17	0.40 ± 0.20
$CK^2_{HP\rightarrow SAP}$(HF)	0.30 ± 0.15	0.31 ± 0.11	0.31 ± 0.18	0.36 ± 0.16
$GSC_{SAP\rightarrow HP}$(LF)	0.063 ± 0.042	0.046 ± 0.043	0.067 ± 0.055	0.044 ± 0.034
$GSC_{HP\rightarrow SAP}$(LF)	0.086 ± 0.047	0.115 ± 0.073	0.084 ± 0.054	0.116 ± 0.069
$GSC_{SAP\rightarrow HP}$(HF)	0.140 ± 0.079	0.119 ± 0.115	0.135 ± 0.073	0.123 ± 0.123
$GSC_{HP\rightarrow SAP}$(HF)	0.068 ± 0.040	0.076 ± 0.038	0.067 ± 0.044	0.082 ± 0.041

CK^2 = causal squared coherence; GSC = Geweke spectral causality; HP = heart period; SAP = systolic arterial pressure; LF = low frequency; HF = high frequency; BAR = bivariate autoregressive model; BDA = bivariate dynamic adjustment model; REST = at rest in supine position; HDT = head-down tilt at −25°. The symbol * indicates a significant difference versus REST with $p < 0.05$ within the same model class (i.e. BAR or BDA).

5.2. Baroreceptor loading reduces the probability of rejecting the null hypothesis of HP-SAP uncoupling along baroreflex

Baroreceptor loading is known to increase vagal modulation, inhibit sympathetic control and increase baroreflex sensitivity (Nagaya *et al* 1995, Weise *et al* 1995, Kardos *et al* 1997, Tanaka *et al* 1999,

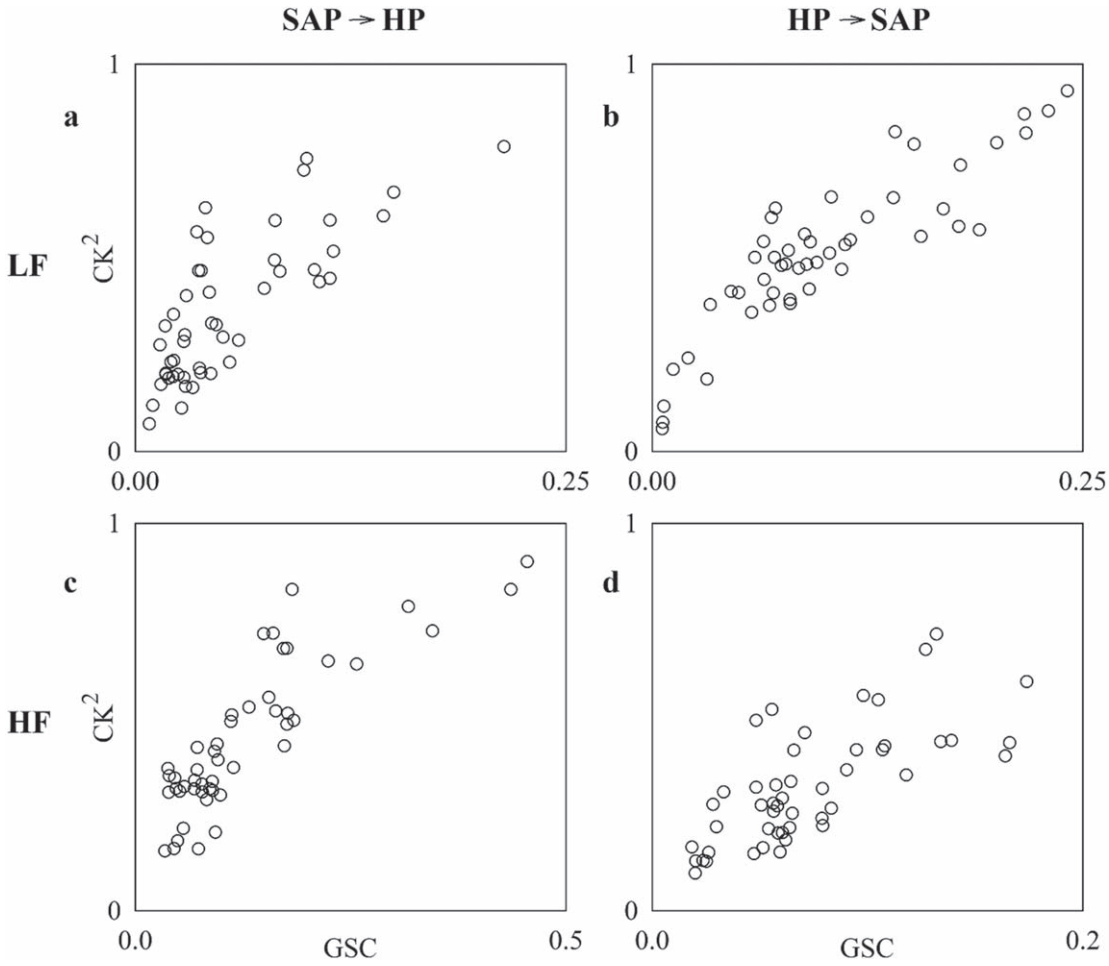

Figure 5. The scatter plots in the plane (GSC, CK^2) show the association between GSC and CK^2. Each open circle corresponds to a pair (GSC, CK^2) in an assigned individual. Data are pooled together regardless of the experimental condition (i.e. REST or HDT) and type of model (i.e. BAR and BDA). The scatter plots are relevant to markers from SAP to HP (a), (c) and from HP to SAP (b), (d) computed in the LF (a), (b) and HF (c), (d) bands.

Cooke *et al* 2003, Porta *et al* 2015a). The major experimental finding of this study is the reduction of the likelihood of rejecting the null hypothesis of HP-SAP uncoupling along the baroreflex during HDT. This result is the consequence of the decrease of the strength of the dependence of HP on SAP (table 1), that makes more difficult to reject the null hypothesis of HP-SAP uncoupling. Remarkably, this result was found in the LF band, namely along time scales typical of the baroreflex control including the resonance frequency of the AP control (De Boer *et al* 1985, Baselli *et al* 1994, Cevese *et al* 2001, Karemaker and Wesseling 2008). The decrease of the strength of baroreflex control is the likely consequence of the decline of the amplitude of SAP oscillations in the LF band (Weise *et al* 1995, Cooke *et al* 2003, Porta *et al* 2015a). The decreased strength of the causal relationship from SAP to HP in the LF band might account for the increased complexity of the HP variability detected in Porta *et al* (2015a). Indeed, SAP variability exhibits a lower complexity compared to HP variability (Porta *et al* 2012b) and a less strong dependence of HP on SAP might lead to increase the HP complexity because HP changes are less importantly driven by regular SAP oscillations and more sensitive to respiratory activity governing HP regardless of SAP (Eckberg 2003). The decrease strength of the causal relationship from SAP to HP was evident using both BAR and BDA models but it became more robust when data were pooled together regardless of the model structure, thus improving the statistical power of the analysis. This conclusion held regardless of the metric utilized to assess the strength of the causal link but CK^2 was slightly more powerful in separating REST and HDT. Conversely, the reduction of the involvement of baroreflex control was not detected in the HF band, thus suggesting that fast oscillations of HP during HDT are less importantly mediated by baroreflex and more related to the activity of respiratory centers able to modulate sinus node responsiveness regardless of baroreflex (Eckberg 2003). Thus, the observed increase of respiratory sinus arrhythmia observed during HDT (Kardos *et al* 1997, Porta *et al* 2015a) could not be completely attributed to baroreflex.

5.3. Baroreceptor loading left unvaried the strength of the link along the mechanical feedforward pathway

At difference from the strength of the dependence of HP on SAP, the one along the reverse causal direction (i.e. from HP to SAP) was not affected by baroreceptor loading. This conclusion is corroborated by table 1 as well. This result is particularly robust because it did not depend on the model structure, metrics exploited to assess spectral causality and time scales. The link from HP to SAP is the result of two opposite tendencies on SAP at the next cardiac beat resulting from the diastolic runoff (Baselli *et al* 1994): (1) a positive effect of the Starling law that tends to increase SAP; (2) a negative influence of the Windkessel effect that tends to decrease SAP. Usually, the strength of the link from HP to SAP is significant in healthy conditions (Porta *et al* 2011, Porta *et al* 2013b) and it was found to decrease in situations of bradycardia, limited HP variability, profound vasodilation, and depressed ventricular contractility such as during general anesthesia with propofol (Porta *et al* 2013a). Therefore, it is not surprising to find out that the HDT did not alter the strength of the dependence of SAP on HP.

5.4. Baroreceptor loading and its impact on the analysis of cardiovascular control mechanisms

Baroreceptor unloading obtained by reducing the venous return to the heart via head-up tilt induces a vagal withdrawal, sympathetic activation, and reduced baroreflex sensitivity (Montano *et al* 1994, Cooke *et al* 1999, Furlan *et al* 2000, Marchi *et al* 2016, De Maria *et al* 2019). The increased involvement of the baroreflex control took the form of an increased strength of the causal link from SAP to HP in the LF band, while no changes were observed in the HF band (Nollo *et al* 2005). Conversely, the present study suggests that the baroreceptor loading induced by HDT produce the opposite effect by decreasing the strength of the causal relationship from SAP to HP. Therefore, we conclude that HDT reduces the relevance of the baroreflex control.

Baroreflex is one of the most important regulatory reflexes in bipedal mammals and contributes importantly to the LF oscillations observed in HP and SAP variability (Karemaker and Wesseling 2008, Baselli *et al* 1994). However, additional control mechanisms contribute importantly to cardiovascular regulations in the LF band (Cohen and Taylor 2002). Among these control mechanisms there are sympathetic rhythm generators of central origin driving slow dynamics of AP and HP (Preiss and Polosa 1974, Ang and Marina 2020) and cardiopulmonary low-pressure reflexes activated by slow modifications of intrathoracic pressure and respiratory activity (Taha *et al* 1995, Hainsworth 2014). The activity of these mechanisms is usually hidden by the dominant action of baroreflex and its resonance properties (Karemaker and Wesseling 2008, Baselli *et al* 1994), thus making difficult their identification and quantification of their contribution to the overall cardiovascular control. The possibility of depowering the role of baroreflex via HDT might favor the study of these mechanisms, the understanding of their role, the evaluation of their relevance and the identification of strategies to potentiate them. This possibility might be particularly of interest to elucidate physiological control mechanisms activated by slow periodical breathing. Given the clinical relevance of LF oscillations in protecting tissue in presence of reduced perfusion and in favoring clearance of interstitial fluid (Anderson and Rickards 2022), the possibility of studying additional mechanisms of LF generation in a condition of depowered activity of one of the most important mechanisms responsible for the genesis of the LF rhythm, namely baroreflex, seems to be particularly relevant. To this purpose directional tools in the frequency domain might play a fundamental role.

5.5. Limitations of the study and future developments

The present study tested the physiological hypothesis that a maneuver loading the baroreceptors limits the contribution of the baroreflex to the HP-SAP closed loop regulation in a gender-homogeneous population. The rationale of enrolling a population comprising solely males is to limit the variability of baroreflex control markers that are known to depend on gender (Laitinen *et al* 2004, Milan-Mattos *et al* 2018) and this dependence underlies the well-known differences in the response of females to orthostatic challenge (Waters *et al* 2002, Grenon *et al* 2006 Barantke *et al* 2008, Catai *et al* 2014). As a likely consequence of the reduced variability of the spectral causality markers, we were able to confirm the physiological hypothesis of the study in a small group of subjects. However, conclusions hold only for males. Future studies should check whether suppositions could be extended even to females and whether conclusions could depend on hormone levels by considering groups before and after menopause.

One possible experimental advancement is grading HDT to verify whether incremental baroreceptor loading could induce a progressive decrement of the baroreflex activation in the LF band and to optimize the inclination of the tilt table to achieve the most relevant effect. Additional methodological improvements could be to test spectral causality approaches grounded on different metrics (Baccala *et al* 1998, Baccala and Sameshima 2001, Chicharro 2011, Faes *et al* 2013a) and to introduce possible confounding factors, such as respiration, that might produce spurious effects on directionality because a quote of HP variability is attributed to the baroreflex whether the confounding input is not included in the analysis (Porta *et al* 2012a).

6. Conclusion

The study applied frequency domain model-based spectral causality markers computed via CK^2 and GSC in connection with a surrogate data test to study cardiovascular control during baroreceptor loading induced by HDT of moderate intensity. We proved that HDT reduces the involvement of baroreflex, and this conclusion holds regardless of the approach and model structure. Findings suggest that the use of HDT to limit the impact of baroreflex and improve the likelihood of observing additional physiological control mechanisms, such as central commands directly acting on the sinus node or modulating AP, that contribute to the complexity of cardiovascular regulation in humans.

Data availability statement

The data cannot be made publicly available upon publication because they contain sensitive personal information. The data that support the findings of this study are available upon reasonable request from the authors.

Authors' contributions

AP, conceived and designed the research; RC performed experiments; AP, BC, VB, FG, and BDM analyzed the data; AP drafted the manuscript; AP prepared the figures; AP, BC, VB, FG, BDM and RC interpreted the results; AP, BC, VB, FG, BDM and RC edited and revised the manuscript; AP, BC, VB, FG, BDM and RC approved the final version of the manuscript.

Funding

Italian Ministry of Health partially supported this study via Ricerca Corrente program to Policlinico San Donato.

Disclosures

No conflicts of interest are declared by the authors.

ORCID iDs

Alberto Porta https://orcid.org/0000-0002-6720-9824
Francesca Gelpi https://orcid.org/0000-0002-9221-6153

References

Akaike H 1968 On the use of a linear model for the identification of feedback systems *Ann. Inst. Stat. Math.* **20** 425–39
Akaike H 1974 A new look at the statistical novel identification *IEEE Trans. Autom. Control* **19** 716–23
Anderson G K and Rickards C A 2022 The potential therapeutic benefits of low frequency haemodynamic oscillations *J. Physiol.* **600** 3905–19
Ang R and Marina N 2020 Low-frequency oscillations in cardiac sympathetic neuronal activity *Front. Physiol.* **11** 236
Baccala L A and Sameshima K 2001 Partial directed coherence: a new concept in neural structure determination *Biol. Cybern.* **84** 463–74
Baccala L A, Sameshima K, Ballester G, Do Valle A C and Timo-Iaria C 1998 Studying the interaction between brain structures via directed coherence and Granger causality *Appl. Signal Process.* **5** 40–8
Barantke M, Krauss T, Ortak J, Lieb W, Reppel M, Burgdorf C, Pramstaller P P, Schunkert H and Bonnemeier H 2008 Effects of gender and aging on differential autonomic responses to orthostatic maneuvers *J. Cardiovasc. Electrophysiol.* **19** 1296–303
Barnett L, Barrett A B and Seth A K 2009 Granger causality and transfer entropy are equivalent for Gaussian variables *Phys. Rev. Lett.* **103** 238701
Barnett L and Seth A K 2014 The MVGC multivariate Granger causality toolbox: a new approach to Granger causality inference *J. Neurosci. Methods* **223** 50–68
Baselli G, Porta A, Rimoldi O, Pagani M and Cerutti S 1997 Spectral decomposition in multichannel recordings based on multi-variate parametric identification *IEEE Trans. Biomed. Eng.* **44** 1092–101
Baselli G, Cerutti S, Badilini F, Biancardi L, Porta A, Pagani M, Lombardi F, Rimoldi O, Furlan R and Malliani A 1994 Model for the assessment of heart period and arterial pressure variability interactions and of respiration influences *Med. Biol. Eng. Comput.* **32** 143–52
Catai A M, Takahashi A C M, Perseguini N M, Milan J C, Minatel V, Rehder-Santos P, Marchi A, Bari V and Porta A 2014 Effect of the postural challenge on the dependence of the cardiovascular control complexity on age *Entropy* **16** 6686–704
Cevese A, Gulli G, Polati E, Gottin L and Grasso R 2001 Baroreflex and oscillation of heart period at 0.1 Hz studied by a-blockade and cross-spectral analysis in healthy humans *J. Physiol.* **531** 235–44

Chen Y, Bressler S and Ding M 2006 Frequency decomposition of conditional Granger causality and application to multivariate neural field potential data *J. Neurosci. Methods* **150** 228–37
Chicharro D 2011 On the spectral formulation of Granger causality *Biol. Cybern.* **105** 331–47
Cohen M A and Taylor J A 2002 Short-term cardiovascular oscillations in man: measuring and modeling the physiologies *J. Physiol.* **542** 669–83
Cooke W H, Hoag J B, Crossman A A, Kuusela T A, Tahvanainen K U O and Eckberg D L 1999 Human responses to upright tilt: a window on central autonomic integration *J. Physiol.* **517** 617–28
Cooke W H, Pellegrini G L and Kovalenko O A 2003 Dynamic cerebral autoregulation is preserved during acute head-down tilt *J. Appl. Physiol.* **95** 1439–45
Corbier C, Chouchou F, Roche F, Barthélémy J-C and Pichot V 2020 Causal analyses to study autonomic regulation during acute head-out water immersion, head-down tilt and supine position *Exp. Physiol.* **105** 1216–22
De Boer R W, Karemaker J M and Strackee J 1985 Relationships between short-term blood pressure fluctuations and heart rate variability in resting subjects: I. A spectral analysis approach *Med. Biol. Eng. Comput.* **23** 352–8
De Maria B, Bari V, Cairo B, Vaini E, Esler M, Lambert E, Baumert M, Cerutti S, Dalla Vecchia L and Porta A 2019 Characterization of the asymmetry of the cardiac and sympathetic arms of the baroreflex from spontaneous variability during incremental head-up tilt *Front. Physiol.* **10** 342
Eckberg D L 2003 The human respiratory gate *J. Physiol.* **548** 339–52
Eichler M 2013 Causal inference with multiple time series: principles and problems *Phil. Trans. R. Soc. A* **371** 20110613
Faes L, Erla S, Porta A and Nollo G 2013a A framework for assessing frequency domain causality in physiological time series with instantaneous effects *Phil. Trans. R. Soc. A* **371** 20110618
Faes L, Nollo G and Porta A 2013b Mechanisms of causal interaction between short-term RR interval and systolic arterial pressure oscillations during orthostatic challenge *J. Appl. Physiol.* **114** 1657–67
Furlan R, Porta A, Costa F, Tank J, Baker L, Schiavi R, Robertson D, Malliani A and Mosqueda-Garcia R 2000 Oscillatory patterns in sympathetic neural discharge and cardiovascular variables during orthostatic stimulus *Circulation* **101** 886–92
Geweke J 1982 Measurement of linear dependence and feedback between multiple time series *J. Am. Stat. Assoc.* **77** 304–13
Grenon S M, Xiao X, Hurwitz S, Sheynberg N, Kim C, Seely E W, Cohen R J and Williams G H 2006 Why is orthostatic tolerance lower in women than in men? Renal and cardiovascular responses to simulated microgravity and the role of midodrine *J. Invest. Med.* **54** 180–90
Hainsworth R 2014 Cardiovascular control from cardiac and pulmonary vascular receptors *Exp. Physiol.* **99** 312–9
Kaminski M, Ding M, Truccolo W A and Bressler S 2001 Evaluating causal relations in neural systems: granger causality, directed transfer function and statistical assessment of significance *Biol. Cybern.* **85** 145–57
Kardos A, Rudas L, Simon J, Gingl Z and Csanády M 1997 Effect of postural changes on arterial baroreflex sensitivity assessed by the spontaneous sequence method and Valsalva manoeuvre in healthy subjects *Clin. Auton. Res.* **7** 143–8
Karemaker J M and Wesseling K H 2008 Variability in cardiovascular control: the baroreflex reconsidered *Cardiovasc. Eng.* **8** 23–9
Laitinen T, Niskanen L, Geelen G, Länsimies E and Hartikainen J 2004 Age dependency of cardiovascular autonomic responses to head-up tilt in healthy subjects *J. Appl. Physiol.* **96** 2333–40
La Rovere M T, Bigger J T, Marcus F I, Mortara A and Schwartz P J 1998 Baroreflex sensitivity and heart-rate variability in prediction of total cardiac mortality after myocardial infarction *Lancet* **351** 478–84
Laude D *et al* 2004 Comparison of various techniques used to estimate spontaneous baroreflex sensitivity (the EuroBaVar study) *Am. J. Physiol.* **286** R226–31
Magagnin V, Bassani T, Bari V, Turiel M, Maestri R, Pinna G D and Porta A 2011 Non-stationarities significantly distort short-term spectral, symbolic and entropy heart rate variability indexes *Physiol. Meas.* **32** 1775–86
Marchi A, Bari V, De Maria B, Esler M, Lambert E, Baumert M and Porta A 2016 Calibrated variability of muscle sympathetic nerve activity during graded head-up tilt in humans and its link with noradrenaline data and cardiovascular rhythms *Am. J. Physiol.* **310** R1134–43
Milan-Mattos J C, Porta A, Perseguini N M, Minatel V, Rehder-Santos P, Takahashi A C M, Mattiello S M and Catai A M 2018 Influence of age and gender on the phase and strength of the relation between heart period and systolic blood pressure spontaneous fluctuations *J. Appl. Physiol.* **124** 791–804
Montano N, Gnecchi-Ruscone T, Porta A, Lombardi F, Pagani M and Malliani A 1994 Power spectrum analysis of heart rate variability to assess changes in sympatho-vagal balance during graded orthostatic tilt *Circulation* **90** 1826–31
Nagaya K, Wada F, Nakamitsu S, Sagawa S and Shiraki K 1995 Responses of the circulatory system and muscle sympathetic nerve activity to head-down tilt in humans *Am. J. Physiol.* **268** H1289–94
Nollo G, Faes L, Porta A, Antolini R and Ravelli F 2005 Exploring directionality in spontaneous heart period and systolic pressure variability interactions in humans: implications in the evaluation of baroreflex gain *Am. J. Physiol.* **288** H1777–85
Ogoh S, Volianitis S, Raven P B and Secher N H 2004 Carotid baroreflex function ceases during vasovagal syncope *Clin. Auton. Res.* **14** 30–3
Pagani M, Montano N, Porta A, Malliani A, Abboud F M, Birkett C and Somers V K 1997 Relationship between spectral components of cardiovascular variabilities and direct measures of muscle sympathetic nerve activity in humans *Circulation* **95** 1441–8
Palus M 1997 Detecting phase synchronisation in noisy systems *Phys. Lett. A* **235** 341–51
Pernice R *et al* 2022 Spectral decomposition of cerebrovascular and cardiovascular interactions in patients prone to postural syncope and healthy controls *Auton. Neurosci.: Basic Clin.* **242** 103021
Pinna G D, Porta A, Maestri R, De Maria B, Dalla Vecchia L A and La Rovere M T 2017 Different estimation methods of spontaneous baroreflex sensitivity have different predictive value in heart failure patients *J. Hypertens.* **35** 1666–75
Pomeranz B *et al* 1985 Assessment of autonomic function in humans by heart rate spectral analysis *Am. J. Physiol.* **248** H151–3
Porta A *et al* 2012b Short-term complexity indexes of heart period and systolic arterial pressure variabilities provide complementary information *J. Appl. Physiol.* **113** 1810–20
Porta A, Bari V, Bassani T, Marchi A, Pistuddi V and Ranucci M 2013a Model-based causal closed loop approach to the estimate of baroreflex sensitivity during propofol anesthesia in patients undergoing coronary artery bypass graft *J. Appl. Physiol.* **115** 1032–42
Porta A, Baselli G and Cerutti S 2006 Implicit and explicit model-based signal processing for the analysis of short term cardiovascular interactions *Proc. IEEE* **94** 805–18
Porta A, Bassani T, Bari V, Pinna G D, Maestri R and Guzzetti S 2012a Accounting for respiration is necessary to reliably infer Granger causality from cardiovascular variability series *IEEE Trans. Biomed. Eng.* **59** 832–41
Porta A, Cairo B, Bari V, Gelpi F, De Maria B and Colombo R 2022 Frequency domain causal interactions between heart period and systolic arterial pressure during baroreflex loading *Proc. of the 12th Conf. of the European Study Group on Cardiovascular Oscillations (ESGCO), 9–12 October 2022 (Štrbské Pleso, Slovakia)* (IEEE Press) (https://doi.org/10.1109/ESGCO55423.2022.9931374)

Porta A, Castiglioni P, Di Rienzo M, Bassani T, Bari V, Faes L, Nollo G, Cividjan A and Quintin L 2013b Cardiovascular control and time domain Granger causality: insights from selective autonomic blockade *Phil. Trans. R. Soc. A* **371** 20120161
Porta A, Catai A M, Takahashi A C M, Magagnin V, Bassani T, Tobaldini E, van de Borne P and Montano N 2011 Causal relationships between heart period and systolic arterial pressure during graded head-up tilt *Am. J. Physiol.* **300** R378–86
Porta A and Faes L 2016 Wiener-Granger causality in network physiology with applications to cardiovascular control and neuroscience *Proc. IEEE* **104** 282–309
Porta A, Faes L, Marchi A, Bari V, De Maria B, Guzzetti S, Colombo R and Raimondi F 2015a Disentangling cardiovascular control mechanisms during head-down tilt via joint transfer entropy and self-entropy decompositions *Front. Physiol.* **6** 301
Porta A, Faes L, Nollo G, Bari V, Marchi A, De Maria B, Takahashi A C M and Catai A M 2015b Conditional self-entropy and conditional joint transfer entropy in heart period variability during graded postural challenge *PLoS One* **10** e0132851
Porta A, Furlan R, Rimoldi O, Pagani M, Malliani A and van de Borne P 2002 Quantifying the strength of linear causal coupling in closed loop interacting cardiovascular variability series *Biol. Cybern.* **86** 241–51
Porta A, Gelpi F, Bari V, Cairo B, De Maria B, Takahashi A C M, Catai A M and Colombo R 2023 Changes of the cardiac baroreflex bandwidth during postural challenges *Am. J. Physiol.* **324** R601–12
Porta Baselli G, Rimoldi O, Malliani A and Pagani M 2000 Assessing baroreflex gain from spontaneous variability in conscious dogs: role of causality and respiration *Am. J. Physiol.* **279** H2558–67
Preiss G and Polosa C 1974 Patterns of sympathetic neuron activity associated with Mayer waves *Am. J. Physiol.* **226** 724–30
Schreiber T and Schmitz A 1996 Improved surrogate data for nonlinearity tests *Phys. Rev. Lett.* **77** 635–8
Shankhwar V, Singh D and Deepak K K 2022 Cardiac-vascular-respiratory coupling analysis during 6-degree head-down tilt microgravity analogue *Biomed. Signal Process. Control* **72** 103358
Smyth H S, Sleight P and Pickering G W 1969 Reflex regulation of the arterial pressure during sleep in man. A quantitative method of assessing baroreflex sensitivity *Circ. Res.* **24** 109–21
Taha B H, Simon P M, Dempsey J A, Skatrud J B and Iber C 1995 Respiratory sinus arrhythmia in humans: an obligatory role for vagal feedback from the lungs *J. Appl. Physiol.* **78** 638–45
Tanaka H, Davy K P and Seals D R 1999 Cardiopulmonary baroreflex inhibition of sympathetic nerve activity is preserved with age in healthy humans *J. Physiol.* **515** 249–54
Taylor J A and Eckberg D L 1996 Fundamental relations between short-term RR interval and arterial pressure oscillations in humans *Circulation* **93** 1527–32
Waters W W, Ziegler M G and Meck J V 2002 Postspaceflight orthostatic hypotension occurs mostly in women and is predicted by low vascular resistance *J. Appl. Physiol.* **92** 586–94
Weise F, London G M, Guerin A P, Pannier B M and Elghozi J-L 1995 Effect of head-down tilt on cardiovascular control in healthy subjects: a spectral analytic approach *Clin. Sci.* **88** 87–93